BBA - Molecular Cell Research 1865 (2018) 1945–1958

Contents lists available at ScienceDirect

BBA - Molecular Cell Research

journal homepage: www.elsevier.com/locate/bbamcr

Clostridium difficile toxin B induces senescence in enteric glial cells: A potential new mechanism of *Clostridium difficile* pathogenesis

Katia Fettucciari[a,*], Lara Macchioni[a], Magdalena Davidescu[a], Paolo Scarpelli[a], Camilla Palumbo[d], Lanfranco Corazzi[a], Andrea Marchegiani[e], Matteo Cerquetella[e], Andrea Spaterna[e], Pierfrancesco Marconi[a], Gabrio Bassotti[b,c]

[a] Department of Experimental Medicine, University of Perugia Medical School, Perugia, Italy
[b] Department of Medicine, University of Perugia Medical School, Perugia, Italy
[c] Gastroenterology and Hepatology Section, Santa Maria della Misericordia Hospital, Perugia, Italy
[d] Department of Clinical Sciences and Translational Medicine, Tor Vergata University, Rome, Italy
[e] School of Biosciences and Veterinary Medicine, University of Camerino, Macerata, Italy

ARTICLE INFO

Keywords:
Enteric glial cells (EGCs)
Clostridium difficile toxin B (TcdB)
Senescence
p27
Sirtuins
JNK
AKT

ABSTRACT

Clostridium difficile infection (CDI) causes nosocomial/antibiotic-associated diarrhea and pseudomembranous colitis, with dramatic incidence/mortality worldwide. *C. difficile* virulence factors are toxin A and toxin B (TcdB) which cause cytopathic/cytotoxic effects and inflammation. Until now studies were focused on molecular effects of *C. difficile* toxins (Tcds) on different cells while unexplored aspect is the status/fate of cells that survived their cytotoxicity. Recently we demonstrated that enteric glial cells (EGCs) are susceptible to TcdB cytotoxicity, but several EGCs survived and were irreversibly cell-cycle arrested and metabolically active, suggesting that EGCs could became senescent. This is important because allowed us to evaluate the not explored status/fate of cells surviving Tcds cytotoxicity, and particularly if TcdB induces senescence in EGCs.

Rat-transformed EGCs were treated with 10 ng/ml TcdB for 6 h–48 h, or for 48 h, followed by incubation for additional 4 or 11 days in absence of TcdB (6 or 13 total days). Senescence markers/effectors were examined by specific assays.

TcdB induces senescence in EGCs, as demonstrated by the senescence markers: irreversible cell-cycle arrest, senescence-associated-β-galactosidase positivity, flat morphology, early and persistent DNA damage (ATM and H2AX phosphorylation), p27 overexpression, pRB hypophosphorylation, c-Myc, cyclin B1, cdc2 and phosphorylated-cdc2 downregulation, Sirtuin-2 and Sirtuin-3 overexpression. TcdB-induced EGC senescence is dependent by JNK and AKT activation but independent by ROS, p16 and p53/p21 pathways.

In conclusion, TcdB induces senescence in EGCs. The extrapolation of these results to CDI leads to hypothesize that EGCs that survived TcdB, once they have acquired a senescence state, could cause irritable bowel syndrome (IBS), inflammatory bowel disease (IBD), and tumors due to persistent inflammation, transfer of senescence status and stimulation of pre-neoplastic cells.

Abbreviations: CDI, *Clostridium difficile* infection; Tcds, toxins of *Clostridium difficile*; TcdA, toxin A of *Clostridium difficile*; TcdB, toxin B of *Clostridium difficile*; EGCs, enteric glial cells; IBS, irritable bowel syndrome; IBD, inflammatory bowel disease; CDKI, cyclin-dependent kinase inhibitors; SA-β-Gal, senescence-associated β-galactosidase; SAHF, senescence-associated heterochromatin foci; SASP, senescence-associated secretory phenotype; phospho-ATM, phosphorylation of Ataxia telangiectasia mutated kinase; γH2AX, phosphorylation of Histone 2AX; cdc2, cell division cycle 2; pRB, phospho-Rb; SIRTs, Sirtuins; JNK, c-Jun N-terminal kinase; AKT, protein-chinasi B; NAC, *N*-acetylcysteine; MnSOD, manganese superoxide dismutase; CDKs, cyclin-dependent kinases; DDR, DNA damage response; DMEM, Dulbecco's Modified Eagle's Medium; FBS, foetal bovine serum; PI, propidium iodide; Ab, antibody; DU, densitometric units; pp53, phospho-p53; DDR, DNA damage response; FOXO, forkhead box-O transcription factors

* Corresponding author at: Department of Experimental Medicine, University of Perugia, Medical School, Lucio Severi Square 1, Bulding B, fourth floor, Sant'Andrea delle Fratte, 06132 Perugia, Italy.
E-mail address: katia.fettucciari@unipg.it (K. Fettucciari).

https://doi.org/10.1016/j.bbamcr.2018.10.007
Received 5 June 2018; Received in revised form 2 October 2018; Accepted 4 October 2018
Available online 06 October 2018
0167-4889/

1. Introduction

Clostridium difficile infection (CDI) is an increasing important infectious disease worldwide with about 500,000 infected subjects per year with approximately 29,000 deaths in the United States and about 124,000 cases in Europe with an overall mortality of 3–30% [1,2]. CDIs represent 15–25% of all opportunistic gastrointestinal infections [1,2]. There has been a dramatic worldwide increase in CDI incidence and mortality mainly due to the emergence of more virulent strains, the ever-widespread use of antibiotics that favour the onset, and the emerging of CDI in populations previously considered at low risk [1,2].

The pathogenic mechanism responsible for CDI is mainly based on the action of two toxins of *C. difficile* (Tcds), toxin A (TcdA) and B (TcdB) with similar molecular structure and mechanism of action but with TcdB being about 1000 times more potent than TcdA [3–5]. Once penetrated inside the cells, both Tcds inactivate by glucosylation the Rho-GTPase, mainly Rac1, RhoA and Cdc42, thus causing disruption of the actin cytoskeleton assembly, cell rounding, loss of adhesion, cell-cycle arrest, apoptosis, or necrosis. At organ level, CDI is manifested with varying degrees of pathology ranging from mild diarrhea to severe life-threatening pseudomembranous colitis [3–5].

With the deepening of cellular damage, which initially involves colonocytes, these Tcds penetrate into the deeper layers of intestinal mucosa [3–5] reaching in the submucosa and myenteric plexus neuronal cells and enteric glial cells (EGCs), that are the major cells regulating gastrointestinal tract physiology [6–8].

While a great contribution of knowledge has been obtained on the molecular effects of Tcds on various cell types [3–5,9], an unexplored aspect is the status and the fate of cells that survived to Tcds effects. This topic could be very important considering our recent *in vitro* results demonstrating that EGCs that survive TcdB have some reduced functions [9] that have led us to speculate that survival *in vivo* of altered EGCs could have functional consequences such as irritable bowel syndrome (IBS) [10]. This speculation was enforced by the demonstration of a significant epidemiological correlation between CDI and the onset of IBS and inflammatory bowel disease (IBD) [11,12]. Therefore, the possibility that altered cells surviving CDI could be responsible for still unknown long-term effects related to the infection is intriguing. To address this problem, we studied the effect of TcdB on EGCs for their key role in the physiology and pathology of gastrointestinal tract [6–8]. Our previous demonstration that EGCs surviving TcdB cytotoxic effects are irreversibly arrested but remain metabolically active [9] suggests that TcdB may induce a senescence state in EGCs.

Cellular senescence induced by various categories of stressors is an acquired new cell state with an irreversible cell-cycle arrest, changes in cell metabolism, morphology, and gene expression [13–21]. Senescent growth arrest is due to induction of cyclin-dependent kinase inhibitors (CDKI) p16, p21, p27 involved in cell-cycle regulatory pathways such as p53/p21, p16/pRb or PTEN/p27 [13–24]. Moreover, other biomarkers such as senescence associated β-galactosidase activity (SA-β-Gal), early and persistent DNA damage response (DDR), senescence-associated heterochromatin foci (SAHF), and senescence-associated secretory phenotype (SASP) have been associated with cellular senescence [13–18]. Contrarily to cellular senescence associated with aging, senescence associated with anti-tumor drugs, irradiation, oxidative stressors, and DNA damaging agents is mediated by external inductors [13–20]. Much attention has been dedicated to the above external inductors due to their widespread use in tumor therapy [13–20]. Some studies also describe senescence associated to toxins produced by bacteria that cause limited infections such as *Escherichia coli* colibactin, *Pseudomonas aeruginosa* pyocyanin, *Streptococcus pneumonie* pneumolysin, cytolethal distending toxin from a subgroup of facultative pathogenic strain of gram- bacteria, and *Salmonella typhi* typhoid toxin [25–30]. However, no information is available on cellular senescence induced by toxins produced by bacteria that cause widely disseminated infections as *Clostridium difficile*.

The senescence state, initially considered a barrier to the development of tumors and an important positive effect of antitumor therapy on resistant tumor cells, is presently considered also a potential dangerous condition due to continued secretion by senescent cells of extremely active molecules that could induce a persistent inflammation, stimulate the proliferation of bystander cells, induce senescence in other cells of the microenvironment, and promote the proliferation of pre-neoplastic cells [13,14,31]. Recently it has been demonstrated the involvement of cellular senescence in several gastrointestinal diseases [32,33].

According to the above considerations and our previous results, the aim of this study was to evaluate whether EGCs that survived TcdB have acquired the senescence state.

This study demonstrated for the first time that TcdB induces senescence in EGCs, as evidenced by the presence of several markers of senescence [13–22,32–34], such as early and irreversible cell-cycle arrest in G1 and G2, SA-β-Gal activity, early increase of phosphorylation of Ataxia telangiectasia mutated kinase (pATM), increase of phosphorylation of Histone 2AX (γH2AX), p27 overexpression, downregulation of cyclin B1 and cell division cycle 2 (cdc2) expression, and hypophosphorylation of phospho-Rb (pRB), downregulation of c-Myc and overexpression of Sirtuins (SIRTs), SIRT2 and SIRT3. Furthermore, we found that TcdB-induced EGC senescence is dependent by c-Jun N-terminal kinase (JNK) and protein-chinasi B (AKT) activation but independent on the p16 and p53/p21 pathways. TcdB induces also early ROS increase in EGCs which is not responsible for senescence induction since their neutralization with *N*-acetylcysteine (NAC) does not affect senescence.

The extrapolation of these *in vitro* results to CDI suggests that EGCs that survived TcdB could transit to a senescence state with an increased risk of disease.

2. Material and methods

2.1. TcdB

TcdB isolated from *C. difficile* strain VPI10463 was obtained from Enzo Life Sciences (BML-G150-0050; Farmingdale, NY), reconstituted to 200 μg/ml stock solution, and stored as indicated in data sheet.

2.2. Cell culture and treatment with TcdB

Rat-transformed EGCs (EGC/PK060399egfr; ATCC® CRL-2690™) [35], obtained from the ATCC (Manassas, VA, USA), were cultured in Dulbecco's Modified Eagle's Medium (DMEM) with 10% foetal bovine serum (FBS), 2 mM L-glutamine, 100 U/ml penicillin, and 100 μg/ml streptomycin (complete medium) at 37 °C with 5% CO_2 for no > 20 passages.

EGCs, for all experiments, were released using 0.05% trypsin-EDTA, plated at 0.5×10^6 cells/well in 2 ml of complete medium on six-well culture plates, and allowed to adhere overnight. Then, the EGCs were treated with TcdB at 10 ng/ml for 6, 24, and 48 h. In some samples TcdB was removed after 48 h and cells were incubated for additional 4 or 11 days (6 or 13 total days). Control and TcdB-treated EGCs were released as described above, washed, and cell viability and total cell numbers were determined by a trypan blue dye-exclusion assay.

In the experiments with JNK inhibitor (SP600125; Cell Signaling, Beverly, MA, USA), AKT inhibitor (perifosine; Cell Signaling), or *N*-acetyl cysteine (NAC; Sigma-Aldrich, Milan, Italy), 10 μM SP600125, 40 μM perifosine or 4 mM NAC were added to EGCs 1 h prior TcdB treatment and maintained during the course of experiments.

In the experiments with etoposide (Sigma-Aldrich), EGCs were treated with 0.1–100 μM etoposide for 6 h.

2.3. MTT assay

EGCs (0.25×10^6 cells/well in 1 ml) were seeded in 12-well plates and treated with TcdB for different times, then MTT was added at 0.5 mg/ml and incubation continued for 2 h at 37 °C. After removal of the medium, 200 µl DMSO was added to each well. Plates were then shaken for 30 min at 37 °C and the absorbance at 550 nm of reduced MTT was measured.

2.4. Cell-cycle evaluation by flow cytometry

Control and TcdB-treated EGCs were recovered at different times, then washed and the 200 ×*g* cell pellets were resuspended in 1 ml of hypotonic fluorochrome solution [propidium iodide (PI) 50 µg/ml in 0.1% sodium citrate plus 0.1% Triton X-100]. The samples were incubated at 4 °C overnight in the dark, and PI fluorescence of individual nuclei was measured by EPICS XL-MCL flow cytometer (Beckman Coulter, FL, USA) to assess the DNA content and detect apoptosis and cell-cycle changes [9,36]. The data were processed by an Intercomp computer and analyzed with EXPO32 software (Beckman Coulter) [9,36]. The cell cycle was examined by measuring DNA-bound PI fluorescence in the orange-red fluorescence channel (FL2) with linear amplification. The percentage of cells in each cell-cycle phase was evaluated with ModFit software (Verity Software House, Topsham, ME, USA) [36].

Apoptosis was analyzed as previously described [9]. The data were processed by an Intercomp computer and analyzed with EXPO32 software (Beckman Coulter).

2.5. SA-β-Gal staining

SA-β-Gal staining was performed according to Dimri et al. [34] using a commercial kit (Cell Signaling) according to the manufacturer's instructions. Images were acquired with inverted phase-contrast microscopy (Orma Scientific) with a MC150C camera and debut video capture software v1.90 (NCH). The percentage of SA-β-Gal positive cells (blue cells) was scored by counting at least 300 cells by randomly choosing 3 microscopic fields under ×20 objective magnification.

2.6. Immunofluorescence

EGCs (0.5×10^6) on cover slips placed in 6 well plates in 2 ml of complete medium were allowed to adhere overnight, then treated with TcdB. At different times, after washing with PBS, the cells were fixed for 20 min with 4% paraformaldehyde and permeabilized for 10 min with 0.1% Triton X-100. Then washed with PBS containing 0.05% Triton X-100 (PBSTr), the cells were incubated for 30 min in blocking buffer (PBSTr containing 2.5% bovine serum albumin). Mouse primary monoclonal antibody (Ab) anti-γH2AX (1:200; Millipore) in blocking buffer was incubated with the cells for 1 h followed by incubation for 1 h with Alexa Fluor 488-labelled goat anti-mouse IgG Ab (1:200; Molecular Probes, Eugene, Oregon, USA) to detect γH2AX [25,28,30]. DAPI (Molecular Probes) was added at 2 mg/ml to counterstain the nuclei. The coverslips were mounted on microscopic glass slides with ProLong Gold antifade medium. All steps were performed at room temperature. Fluorescence microscopy images were captured using an Axio Observer.Z1 microscope with ApoTome 2 and AxioCam MRm camera (Carl Zeiss Microscopy), and a 63×/0.75 oil immersion NEOFLUAR objective. Z-axis volume of cells was entirely covered capturing 0.30 µM spaced focal planes. Images were deconvolved using ZEN software (Carl Zeiss Microscopy); cleaned Z-stacks of images were used to realize extended depth of focus flat projections from the 3D object. DAPI grayscale sub-channel was converted into red color. Resulting images were individually analyzed using ZEN software built-in plugin for colocalization. A fluorescence threshold was set at a high cutoff value of 10,000 in the Alexa Fluor 488 channel and positive pixels above the given threshold were automatically counted by the software. For each image, number of positive pixels above the threshold was normalized considering the number of nuclei present in the corresponding frame and data were plotted.

2.7. Western blot analysis

Control and TcdB-treated EGCs were lysed at different times with a modified RIPA buffer containing protease and phosphatase inhibitors (Sigma-Aldrich). Control and Etoposide-treated EGCs were lysed at 6 h with a modified RIPA buffer containing protease and phosphatase inhibitors (Sigma-Aldrich). Protein content was determined by a standard Bradford protein assay (Bio-Rad Laboratories, Milan, Italy). Proteins (20 µg) were separated on 6%, 10% or 12% SDS-PAGE and transferred to nitrocellulose membranes, which were blocked and then incubated overnight at 4 °C with primary Abs to the following: p21 (WAF/Cip1; affimetrix, Invitrogen, Milan, Italy); p15/16 (C-7), ATM (1B10) and β-actin (Santa Cruz Biotechnology, Santa Cruz, CA, USA); p27, cyclin B1, cyclin D1, cyclin D3, cdc2, phospho-cdc2 (Thr161) phospho-cdc2 (Tyr15), SIRT1–7, phospho-Rb (Ser795; pRb), phospho-JNK (Thr183/Tyr185; pJNK), phospho-AKT (Ser473; pAKT), AKT, PTEN, p53, phospho-p53 (Ser15) (Cell Signaling Technology); MnSOD and Rac1 (clone 102) (Upstate Biotechnology, Lake placid, NY, USA) phospho-ATM (Ser1981; pATM) (Merck, Rome, Italy) [9,22–24]. Signals were detected with horseradish peroxidase-conjugated secondary antibodies and the enhanced chemiluminescence system (GE Healthcare, Milan, Italy). Membranes were stripped with 0.2 M NaOH in double-distilled water for 15 min, washed, and reprobed. β-Actin was used as loading control. One experiment representative of four independent experiments is shown. Densitometric analysis was performed after scanning by Quantity One software (Bio-Rad Laboratories). The results are expressed as arbitrary densitometric units (DU) relative to the densitometric units of β-actin from four independent experiments. The data were analyzed by Student's *t*-test.

2.8. Fluorescent determination of ROS

EGCs were treated with TcdB in serum- and phenol red-free DMEM, and then stained for 30 min at 37 °C with fluorescent probes prior to harvesting. Total intracellular ROS were determined by 5-(and 6)-chloromethyl-2′,7′-dichlorohydrofluorescein diacetate (CM-H2DCFDA,10 µM; Molecular Probes, Invitrogen, Italy) (λ exc 485 nm, λ em 535 nm).

2.9. Catalase activity

Catalase activity was determined in EGCs pellet solubilized with 1% Triton X-100 by measuring the rate of decomposition of H_2O_2 at 240 nm for 5 min according to Aebi HE [37]. The decrease in absorbance of H_2O_2 was measured as triplicates and catalase activity was expressed as µmol H_2O_2/min/10^6 cells, calculated using a molar extinction coefficient of 39.4 M^{-1} cm^{-1}.

3. Results

3.1. TcdB induces persistent cell-cycle arrest in EGCs

Previously we demonstrated that in EGCs TcdB causes early cell-cycle arrest and cells that resist apoptosis survive for up to 13 days without proliferative activity, but metabolically active [9]. These results suggest that TcdB may induce a state of senescence in ECGs, because a key hallmark of senescence is the irreversible exit from the cell-cycle [13–17,33]. Therefore, to define the characteristic of cell-cycle arrest in deeper, we first evaluated the proliferative activity of EGCs treated with TcdB for 6–48 h, or for 48 h, followed by incubation for additional 4 or 11 days in the absence of TcdB (6 or 13 total days), by

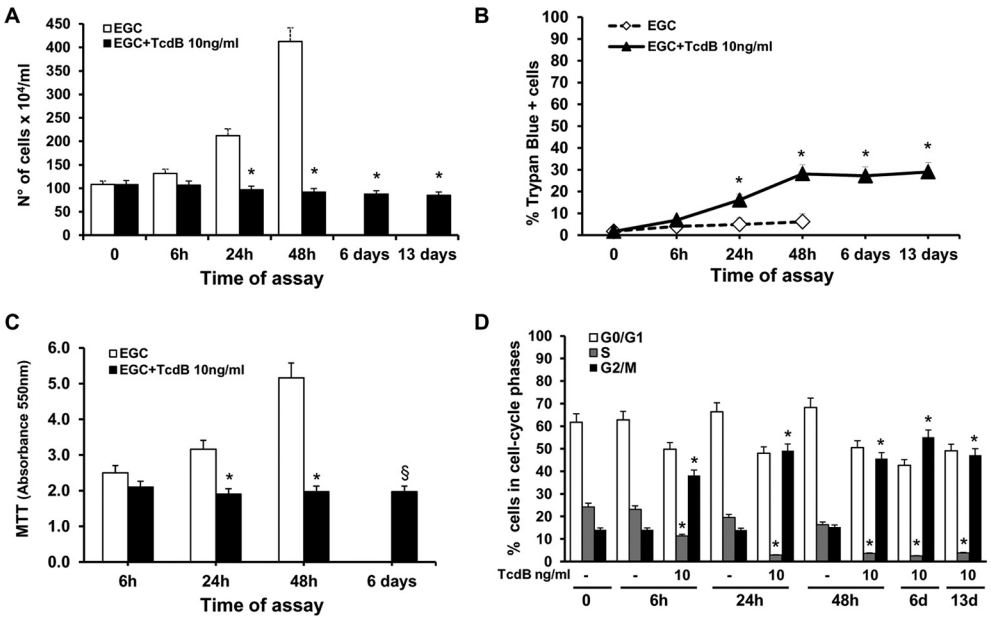

Fig. 1. Effect of TcdB on EGC cell growth. Control and TcdB-treated EGCs were recovered at the times indicated and was determined: the total cell number (A) or the percentage of trypan blue positive cells (B), by trypan blue assay; (C) the cell viability by MTT; (D) the percentages of cells in the cell-cycle phases by flow cytometry with ModFit software.
Data are the mean ± standard deviation of seven experiments performed in triplicate.
In A, B, D, *P < 0.01, TcdB-treated *versus* control EGCs at time 0, Student's *t*-test.
In C, *P < 0.01, TcdB-treated EGCs *versus* respective control EGCs, and §P < 0.01, TcdB-treated EGCs at 6 days *versus* control EGCs at 48 h, Student's *t*-test.

trypan blue assay, MTT assay, and flow cytometry analysis of DNA content after PI staining.

We confirmed that TcdB-treated EGCs were immediately (6 h) and persistently (6 and 13 days) growth arrested, while untreated cells grew exponentially, being tightly confluent already at 48 h (Fig. 1A). The viability of TcdB-treated EGCs was reduced of about 28% at 48 h and remaining essentially unchanged until 13 days (Fig. 1B). MTT assay showed that TcdB causes a rapid and irreversible arrest of cell proliferation (Fig. 1C). PI staining showed early and persistent cell-cycle arrest in G0/G1 and G2/M phases accompanied by a decrease of cells in the S phase (Fig. 1D). Cell-cycle arrest in G2/M phase at difference of G0/G1 was progressive, indeed was evident at 6 h and reached a maximum at 24 h that persisted until 13 days (Fig. 1D).

Altogether these results indicate that TcdB induces in EGCs an early cell-cycle arrest both in G1 and G2 phases that persists in EGCs that survived to TcdB.

3.2. TcdB induces SA-β-Gal activity in EGCs

Since an important marker of senescence is the increase of SA-β-Gal activity at pH 6 [13–17,32–34], we evaluated SA-β-Gal activity during 13 days after TcdB treatment.

In control EGCs, SA-β-Gal positive cells did not exceed 3 ± 1% at 24 and 48 h (Fig. 2A and B). In TcdB-treated EGCs, 7 ± 1% cells were SA-β-Gal positive in the same time interval (Fig. 2A and B). The percentage of SA-β-Gal positive increased to about 93 ± 3% at 6 and 13 days (Fig. 2A and B), with several cells exhibiting a flat, enlarged morphology (Fig. 2A).

3.3. TcdB induces early and persistent DNA damage

Several studies have shown a causal link between DDR and senescence induction [13–17,30,38]. Formation and persistence of DNA damage foci containing γH2AX is recognized as an indicator for DNA damage and activation of DDR [13–17,38]. Consequently γH2AX staining is established as a reliable quantitative indicator of DNA damage associated with senescence induction [13–17,30,38]. Accordingly, to evaluate whether TcdB induces persistent DNA damage, we analyzed control and TcdB-treated EGCs at 6 h–13 days for the presence of nuclear foci positive for γH2AX *via* DAPI and γH2AX co-staining.

The immunofluorescence analysis showed in TcdB-treated cells a significant increase in the size and intensity of γH2AX foci already at 6 h that persisted at 6 and 13 days (Fig. 3A). Analysis of the γH2AX pixel for nuclei confirmed already at 6 h two-fold higher γH2AX fluorescence, which decreased at 48 h and then persisted unchanged until 13 days, remaining anyway in TcdB-treated EGCs significantly higher than in control at 48 h (Fig. 3B). Moreover, already at 6 h the nuclei of TcdB-treated EGCs became smaller and increased chromatin condensation (Fig. 3A).

To evaluate if the strong induction of γH2AX very early after intoxication (6 h) much before the acquisition of the senescent phenotype, is associated with induction of some type of DNA damage [13–17,38] we evaluated the levels of phosphorylation of the kinase ATM in control and TcdB-treated EGCs at 1.5 h–6 days by Western blot.

TcdB induces in EGC an early and strong phosphorylation of ATM at 1.5 h that remained phosphorylated at lower levels until to 48 h but increase again at 6 days (Fig. 4A).

Since the kinetics of TcdB-catalysed Rac and Rho glucosylation at the specific Thr37 (RhoA) or Thr35 (Cdc42 and Rac1) residues [3–5,9,39,40], are almost identical [3–5,9,39,40], the Western blot to non-glucosylated Rac1 is ideal for assessing the UDP glucosylation of the Rho GTPases by TcdB [39,40]. Therefore, to confirmed, as previously demonstrated [9], that TcdB cause the UDP glucosylation of the Rho GTPases and their kinetics, we analyzed Rac1 glucosylation by Western blot in lysates from control EGCs and EGCs treated with 10 ng/ml TcdB for 1.5 h–13 days using an antibody that recognizes non-glucosylated Rac1 (anti-Rac1 clone 102) [39,40].

TcdB induced a strong reduction of recognition of Rac1 by anti-Rac1 clone 102 indicative of Rac1 glucosylation [39,40] already at 1.5 h which persisted also at 13 days (Fig. 4B). In particular, TcdB at 10 ng/ml induced already at 1.5 h approximately 90% Rac1 glucosylation (Fig. 4B).

3.4. Mechanisms of TcdB-induced permanent cell-cycle arrest in EGCs

The irreversible cell-cycle arrest that characterizes cellular senescence involves cell cycle inhibitors, including p53, pRb, PTEN, c-Myc, and the CDKI (p21, p15/16, and p27), through three main pathways, *i.e.* the p53/p21, p16/pRb, or PTEN/p27, any CDKI pathway exhibiting a prominent role according to stressor and/or cell type [13–24,41].

To define the mechanisms involved in TcdB-induced senescence, we analyzed the expression levels of the main cell cycle inhibitors and of the major regulatory proteins (cyclins and CDKs) of G2/M cell-cycle phase in control and TcdB-treated EGCs at 6 h–13 days.

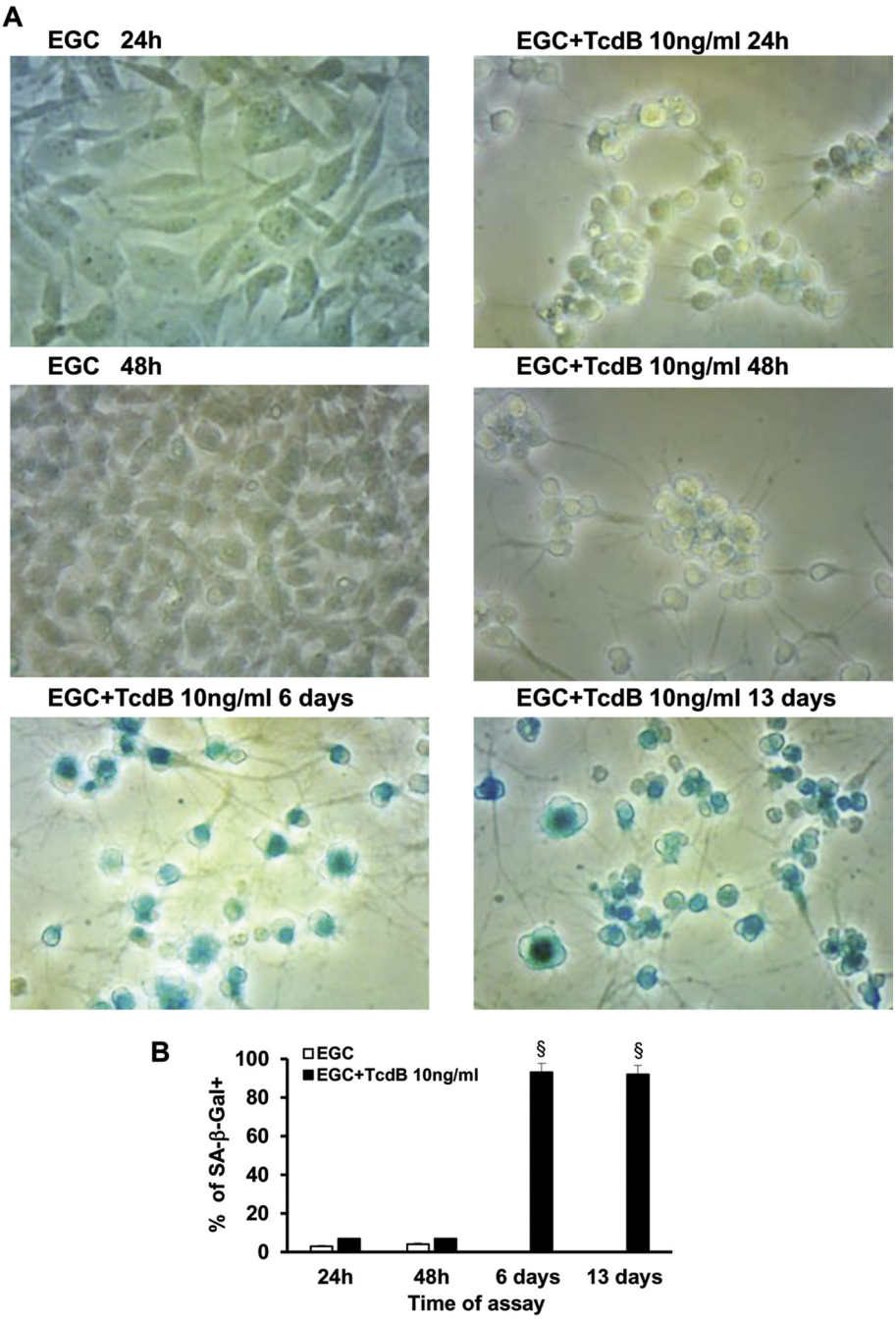

Fig. 2. TcdB induces SA-β-Gal activity in EGCs.
(A) Representative micrographs (200× magnification) of control and TcdB-treated EGCs submitted to SA-β-Gal activity assay at the times indicated. Senescent cells are stained in blue. (B) The graph shows the percentage of SA-β-Gal positive cells in each experimental condition. Data are the mean ± standard deviation of four independent experiments performed in duplicate. $^{§}P < 0.01$, TcdB-treated EGCs at 6 or 13 days *versus* control EGCs at 48 h, Student's *t*-test.

In TcdB-treated EGCs p27 levels were significantly increased already at 6 h, further increased until 48 h, and persisted until 13 days, whereas PTEN levels were not significantly changed at all time examined (Fig. 5A). The p21 increased significantly at 48 h and persisted higher until 13 days (Fig. 5B). The levels of p15/16 were significantly lower at 48 h and further decreased until 13 days (Fig. 5C), whereas pRb levels decreased sharply from 24 h until 13 days (Fig. 5D). Cyclin D1 and cyclin D3 levels were not affected at all time examined (data not shown). The regulators of G2/M phase, cyclin B1 (Fig. 5E), cdc2 (Fig. 5F), phosho-cdc2 Thr161 and phosho-cdc2 Tyr15 (Fig. 5G) were strongly decreased at 24 h and continued to further decrease until 6 days (Fig. 5E–G). Moreover, for phosho-cdc2 Tyr15 there was an accumulation of the inactive hyperphosphorylated form of cdc2 Tyr 15 (the upper band) (Fig. 5G), consistent with the G2 arrest. c-Myc levels were decreased already at 6 h and persisted lower until 6 days (Fig. 5H).

Although rat-transformed EGCs [35] are considered similar to rat primary EGCs [35,42], and have functional properties similar to human EGCs [42], to check if the p53 pathway is still functional [43–45] in these immortalised cells, we induce DNA damage in EGC with etoposide at 0.1–100 μM for 6 h and looking as functionality parameter the phosphorylation and expression/stabilization of p53 by Western blot [43–45].

Western blot analysis shows that etoposide induces in EGCs phosphorylation and stabilization of p53 in a dose dependent manner

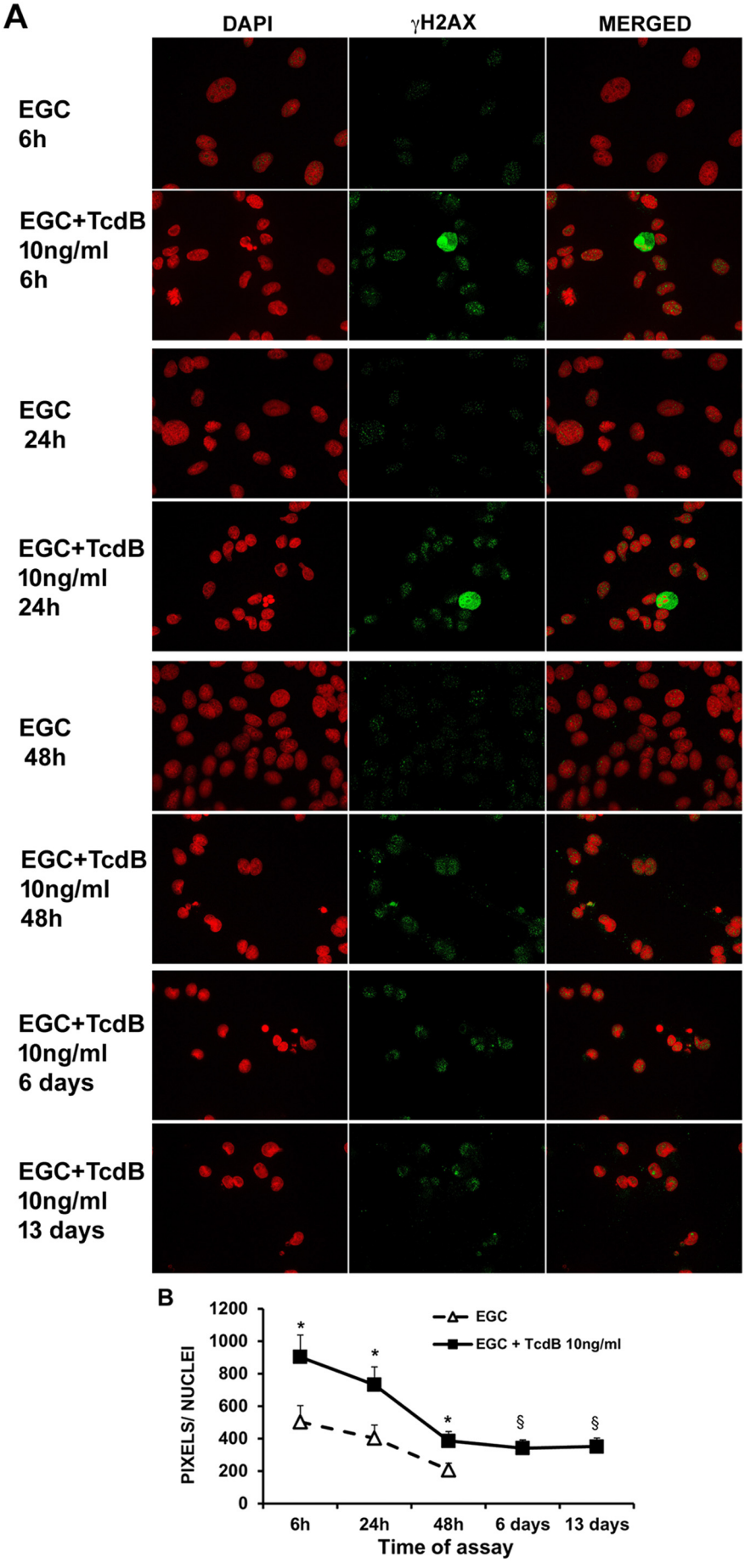

(caption on next page)

Fig. 3. TcdB increases γH2AX staining in EGCs.
(A) At the indicated times, control and TcdB-treated EGCs were immunolabelled with γH2AX (green), using DAPI (converted to red) to counterstain cell nuclei. Images captured from one experiment as described in Material and methods, are representative of three independent experiments. (B) The graph shows the mean ± standard deviation of the pixels/nuclei, scored as described in Material and methods, obtained in three independent experiments. *P < 0.01, TcdB-treated EGCs *versus* respective control EGCs, and §P < 0.01, TcdB-treated EGCs at 6 or 13 days *versus* control EGCs at 48 h, Student's *t*-test.

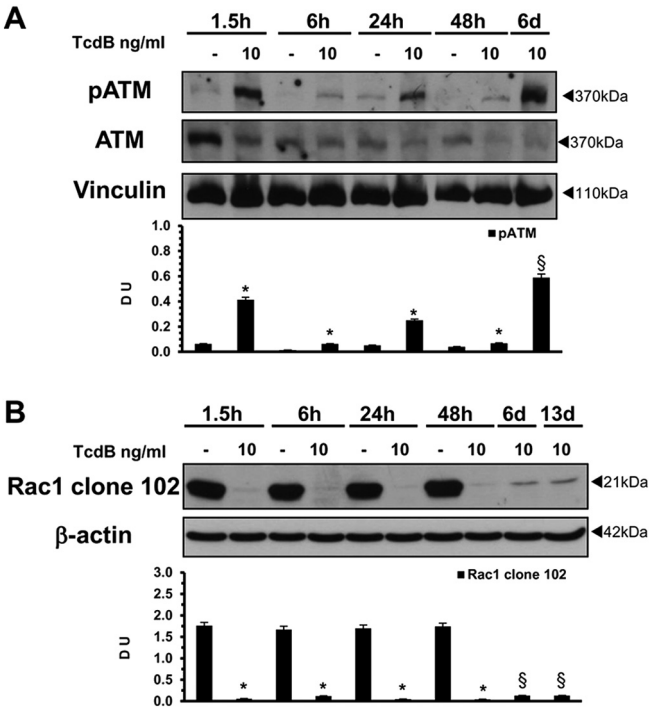

Fig. 4. TcdB induces early phosphorylation of ATM and early and persistent glucosylation of Rac1.
Lysates from control and TcdB-treated EGCs prepared at the indicated times were subjected to SDS-PAGE. (A) The filter was probed with anti-phospho-ATM (Ser1981; pATM) then stripped and probed with anti-vinculin, then with anti-ATM after stripping. The graph represents the densitometric analysis of pATM relative to vinculin. *P < 0.01, TcdB-treated EGCs *versus* respective control EGCs, and §P < 0.01, TcdB-treated EGCs at 6 days *versus* control EGCs at 48 h, Student's *t*-test. (B) The filter was probed with anti-Rac1 clone 102 then stripped and probed with anti-β-actin. The graph represents the densitometric analysis of Rac1 clone 102 relative to β-actin. *P < 0.01, TcdB-treated EGCs *versus* respective control EGCs, and §P < 0.01, TcdB-treated EGCs at 6 or 13 days *versus* control EGCs at 48 h, Student's *t*-test.

(Fig. 6). In fact, at 6 h phopho-p53 levels strong increased already with 0.1 μM etoposide, further increased with 1–10 μM and reaching the maximum increased with 100 μM (Fig. 6A). Regarding the p53 expression levels they were increased of about 2.4-fold with 0.1–1 μM, about 3.6-fold with 5–10 μM and reaching the maximum increased (about 6.8-fold) with 100 μM (Fig. 6B).

Altogether these results indicate that TcdB-induced cell-cycle arrest in EGCs is characterized by strong p27 increase and downregulation of cyclin B1 and cdc2 crucial in G2/M transition without involvement of p16/pRB and p53/p21 axis.

3.5. ROS are not involved in TcdB-induced senescence in EGCs

ROS play important roles in senescence [14–16,20,25,29,46]. Since we have previously demonstrated that TcdB induces ROS generation in EGCs [47], we evaluated whether ROS were involved in TcdB-induced EGCs senescence. To this end, we examined the time course (6 h–13 days) of intracellular ROS levels by labelling EGCs with dichlorofluorescein (CM-H2DCFDA).

Intracellular ROS levels were 2.2-fold higher in TcdB-treated EGCs at 6 h and increased to 8.5-fold at 48 h, then went back to control levels at 6 and 13 days (Fig. 7A). The ROS scavenger NAC [29,46–48], added 1 h before treatment with TcdB for 48 h and maintained during the course of experiments, did not change the percentage of SA-β-Gal positive cells in TcdB treated-EGCs at 13 days (Fig. 7B), as compared to the cells treated with TcdB alone (Fig. 7B), indicating that ROS do not play a key role in our senescence model.

Since the decrease of intracellular ROS levels in TcdB-treated EGCs at 6 and 13 days could be due to upregulation of an antioxidant response by induction of the ROS scavengers, MnSOD and catalase [48–52], we analyzed at 6 h–13 days the expression of MnSOD by Western blot, and catalase activity by enzymatic assay.

MnSOD expression levels in TcdB-treated EGCs increased by 1.5-fold at 24 h, 2.8-fold and 48 h, and reached about 4.6-fold increase at 13 days (Fig. 7C). Catalase activity peaked at 24 and 48 h in TcdB-treated EGCs but returned to control value at 6 and 13 days (Fig. 7D).

Altogether these data indicate that TcdB induces in EGCs ROS generation that is contrasted by an antioxidant response.

3.6. TcdB induces overexpression of SIRT2 and SIRT3 in EGCs

SIRTs, a class of seven members (SIRT1–7) with histone deacetylase or mono-ribosyltransferase activity, are involved in many biological processes including senescence, with either senescence promoting or preventing role in different cell types, by regulation of p27, MnSOD, catalase, and other molecules involved in control of cell-cycle, DNA damage repair, apoptosis, and management of ROS [38,49–52].

Since p27 overexpression (Fig. 5A) and antioxidant response (Fig. 7C and D) could be the result of SIRTs activity, we investigated whether SIRTs were involved in TcdB-induced senescence by evaluating the expression of SIRT1–7 by Western blot.

In TcdB-treated EGCs, SIRT3 and SIRT2 expression levels were significantly higher at 24 h and further increased until 13 days, with SIRT3 (28 kDa; Fig. 8A) reaching a 3-fold and SIRT2 (39 kDa; Fig. 8B) a 4-fold increase. At 6 and 13 days, the 43 kDa isoform of SIRT2 was also strongly increased (Fig. 8B). SIRT6 increased significantly at 6 and 13 days (Fig. 8A), and SIRT5 increased significantly at 6 days (Fig. 8C). In contrast, SIRT1 and SIRT7 levels were not significantly changed at all the examined times (Fig. 8A and D).

These results suggest that particularly SIRT2 and SIRT3 could be involved in TcdB-induced senescence in EGCs.

3.7. JNK activation is involved in TcdB-induced EGC senescence

JNK signalling pathway is frequently involved in senescence induction by several mechanisms, including nuclear import and activation of forkhead box-O transcription factors (FOXO) and transcription of their target genes (*e.g.* p27, MnSOD and catalase) [15,19,20,29,52]. The observation that TcdB induces strong and persistent increase of p27 (Fig. 5A), MnSOD and catalase (Fig. 7C and D), and the previous demonstration that TcdB activates in EGCs JNK during the first 24 h [47], led us to examine whether JNK signalling is involved in TcdB-induced EGC senescence. To this, we examined JNK activation in control and TcdB-treated EGCs at 6 h–6 days by Western blot, and the effect of the JNK inhibitor, SP600125 [47], in a detailed time kinetic on: a) JNK phosphorylation and p27 expression by Western blot analysis, b) viability by evaluation of cell number/viability by trypan blue assay and apoptosis by measuring changes in DNA content *via* flow cytometry [9].

The phosphorylation of 46 kDa JNK showed just increased levels in

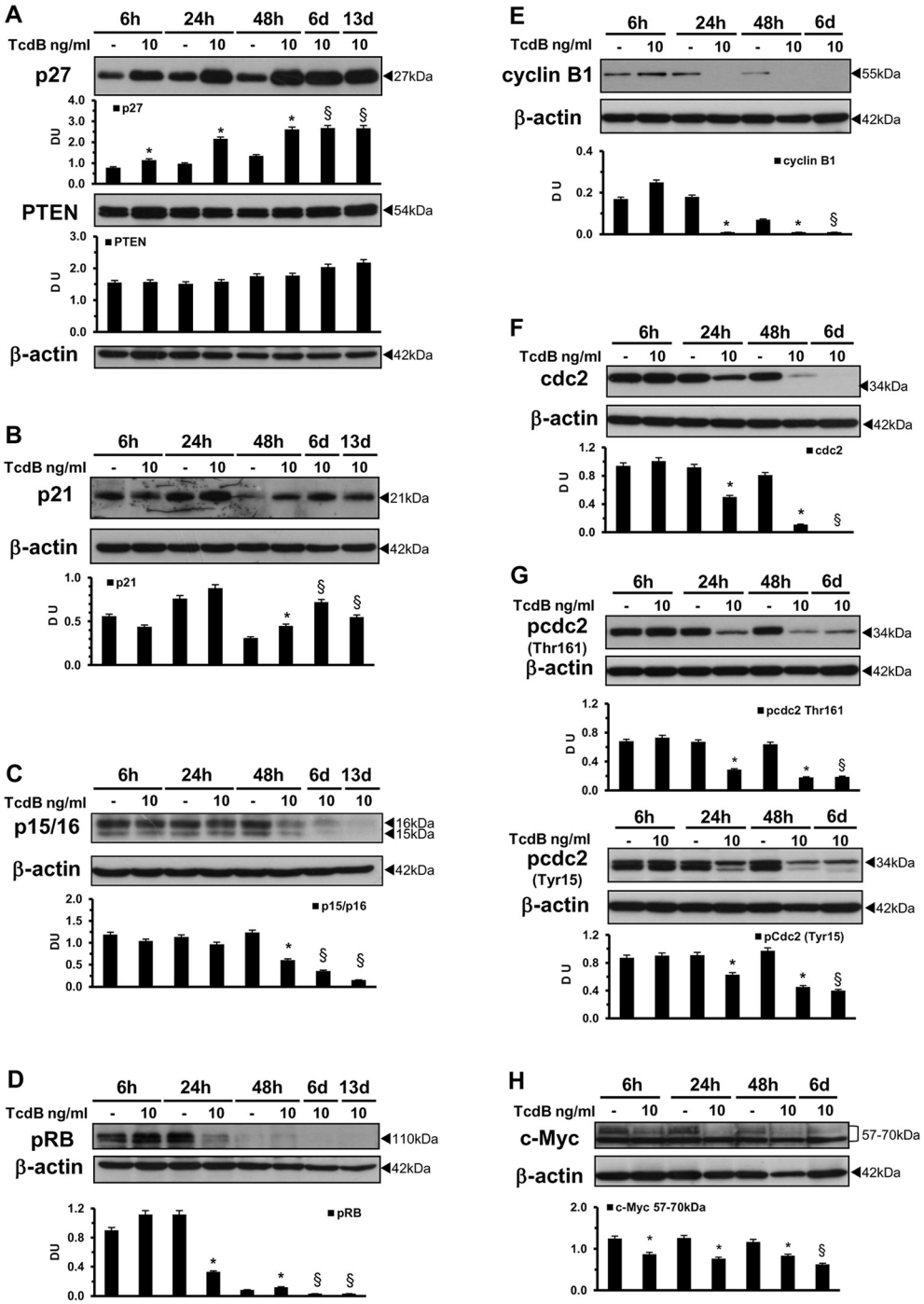

Fig. 5. Molecular mechanisms of cell-cycle arrest in TcdB-induced EGC senescence.
Lysates from control and TcdB-treated EGCs prepared at the indicated times were subjected to SDS-PAGE. (A) The filter was cut around 35 kDa to probe the bottom section with anti-p27 and top section with anti-β-actin, then the top section was stripped and probed with anti-PTEN. (B) The filter was cut around 35 kDa to probe the bottom section with anti-p21 and the middle section with anti-β-actin. (C) The filter was probed with anti-p15/16, then stripped and probed with anti-β-actin. (D) The filter was cut around 70 kDa to probe the top section with anti-pRB and the middle section with anti-β-actin. (E) The filter was probed with anti-β-actin, then stripped cut around 30 kDa and the top section probed with anti-cyclin B1. (F) The filter was probed with anti-cdc2, then stripped and probed with anti-β-actin. (G) The filters were probed with anti-phosho-cdc2 (pcdc2) (Thr161) or with anti-phosho-cdc2 (pcdc2) (Tyr15) then stripped and probed with anti-β-actin. (H) The filter was cut around 35 kDa to probe the top of section with anti-c Myc then the top section was stripped and probed with anti-β-actin.
The graphs represent the densitometric analysis of each protein relative to β-actin. *P < 0.01, TcdB-treated EGCs *versus* respective control EGCs, and §P < 0.01, TcdB-treated EGCs at 6 or 13 days *versus* control EGCs at 48 h, Student's *t*-test.

TcdB-treated EGCs at 6 h with a tendency to increase until 6 days while phosphorylation of 54 kDa JNK was increased at 24 h with a tendency to increase until 6 days (Fig. 9A).

SP600125 reduced in TcdB-treated EGC the JNK phosphorylation at all time examined (Fig. 9B and C) and expression of p27 at 24 and 48 h (Fig. 9B) while induce cell death progressively from 48 h to 6 days as demonstrated by the percentage of trypan blue positive cells and apoptosis (Fig. 9D and E). In fact, pretreatment with SP600125 increased the percentage of trypan blue positive cells progressively by approximately 2-fold at 72 h (28.3 ± 2.7% in TcdB-treated EGCs *versus* 54.4 ± 3.9% in TcdB-treated EGC plus SP600125) (Fig. 9D lines) until to 2.6-fold at 6 days (30.7 ± 3.2% in TcdB-treated EGCs *versus* 81.2 ± 3.7% in TcdB-treated EGC plus SP600125) (Fig. 9D lines). Regarding the percentage of apoptotic cells, SP600125 at 24 h inhibits of about 35% TcdB-induced apoptosis in EGC (Fig. 9E), as previously demonstrated also by Macchioni et al. [47], but then increased the percentage of apoptotic cells from 25.6% ± 2.2% in TcdB-treated EGCs to 34.6 ± 2.9% in TcdB-treated EGCs plus SP600125 at 48 h (about 1.3-fold) (Fig. 9E), from 23.1 ± 1.9% in TcdB-treated EGCs to 47.6 ± 3.3% in TcdB-treated EGCs plus SP600125 at 72 h (about 2-fold) (Fig. 9E), from 21.9 ± 1.4% in TcdB-treated EGCs to 50.8 ± 3.5% in TcdB-treated EGCs treated plus SP600125 at 96 h (about 2.3-fold) (Fig. 9E), and from 16.7 ± 1.2% in TcdB-treated EGCs to 53.2 ± 2.5% in TcdB-treated EGCs plus SP600125 at 6 days (about 3.2-fold) (Fig. 9E).

Altogether these data suggest that JNK is partially involved in induction of p27 and contribute to the survival of EGCs and particularly the observation that EGC treated with JNK inhibitor start to die

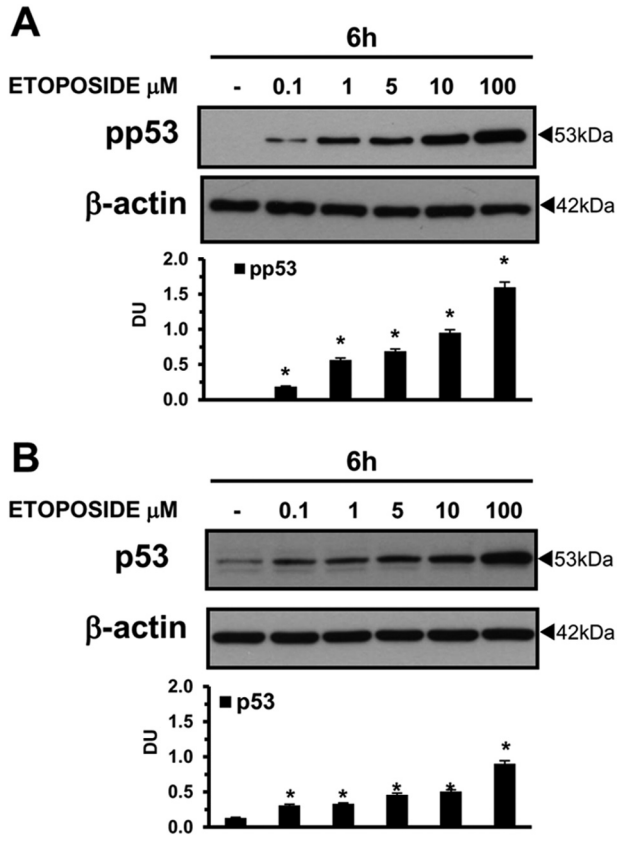

Fig. 6. Effect of etoposide on p53 pathway in EGC.
Lysates prepared from control EGCs and EGCs treated with etoposide 0.1–100 μM for 6 h were subjected to SDS-PAGE. (A) The filter was probed with anti-phospho-p53 (Ser15; pp53) then stripped and probed with anti-β-actin. (B) The filter was probed with anti-p53 then stripped and probed with anti-β-actin. The graphs represent the densitometric analysis of each protein relative to β-actin. *P < 0.01, etoposide-treated EGCs *versus* control EGCs.

between 48 h and 72 h suggests that TcdB treated EGC make the choice between apoptosis or senescence between 48 h and 72 h.

3.8. AKT activation is involved in TcdB-induced EGC senescence

Since recent reports have shown that AKT activation is involved in senescence regulation by several mechanisms [24,52,53], we evaluated the activation of AKT in control and TcdB-treated EGCs at 6 h–6 days by Western blot, and the effect of the AKT inhibitor, perifosine [54,55], on: a) AKT phosphorylation by Western blot analysis, b) viability by evaluation of cell number/viability by trypan blue assay and apoptosis by measuring changes in DNA content *via* flow cytometry [9].

AKT phosphorylation was increased in TcdB-treated EGCs with respect to control cells at all time examined, with the higher level at 6 h (Fig. 10A), suggesting its involvement in senescence. The AKT inhibitor perifosine prevents the AKT phosphorylation already at 6 h (Fig. 10B), and it induced massive cell death already at 48 h (Fig. 10C and D). In fact, pretreatment with perifosine increased the percentage of trypan blue positive cells by 2.2-fold already at 48 h (29.4 ± 2.4% in TcdB-treated EGCs *versus* 64.8 ± 3.4% % in TcdB-treated EGC plus perifosine) (Fig. 10C lines) and this increased of cell death was maintained until 6 days (34.3 ± 2.5% in TcdB-treated EGCs *versus* 77.2 ± 3.2% in TcdB-treated EGC plus perifosine) (Fig. 10C lines). Regarding the percentage of apoptotic cells, evaluated by measuring changes in DNA content *via* flow cytometry, pretreatment with perifosine increased the percentage of apoptosis from 24.2 ± 2.9% in TcdB-treated EGCs to 38.8 ± 3.6% in TcdB-treated EGCs plus perifosine at 48 h (about 1.6-fold) (Fig. 10D), from 22.7% ± 2.3% in TcdB-treated EGCs to 46.8 ± 3.1% in TcdB-treated EGCs plus perifosine at 72 h (2-fold) (Fig. 10D), from 20.9% ± 1.5% in TcdB-treated EGCs to 57.0 ± 2.7% in TcdB-treated EGCs treated plus perifosine at 96 h (about 2.7-fold) (Fig. 10D), and from 15.6% ± 1.4% in TcdB-treated EGCs to 74.2 ± 3.2% in TcdB-treated EGCs plus perifosine at 6 days (4.7-fold) (Fig. 10D).

These data indicate that AKT is strongly involved in induction of senescence by favouring survival of TcdB-treated EGCs and in particular to make the choice between apoptosis or senescence.

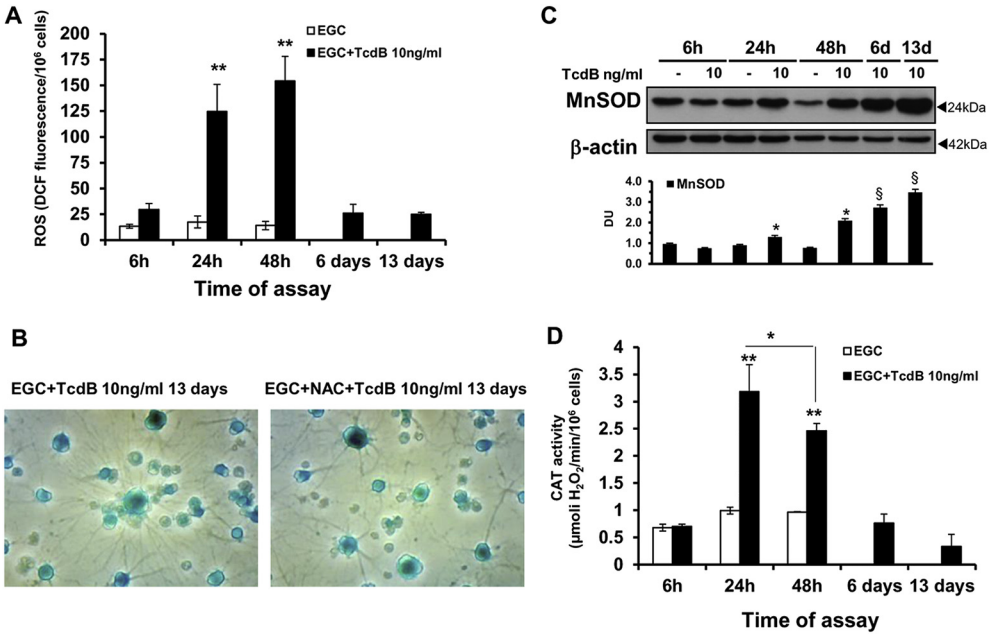

Fig. 7. Role of ROS in TcdB-induced EGC senescence.
(A) Fluorimetric quantitation of total ROS by staining with 10 μM CM-H2-DCFDA. Data are expressed as DCF fluorescence/10^6 cells. (B) Representative micrographs (200× magnification) of TcdB-treated EGCs pre-treated with NAC and TcdB-treated EGCs non-treated with NAC submitted to SA-β-Gal activity assay at 13 days. Senescent cells are stained in blue. (C) The filter was cut around 35 kDa to probe the top section with anti-β-actin and bottom section with anti-MnSOD after stripping.
The graph represents the densitometric analysis of MnSOD relative to β-actin. *P < 0.01, TcdB-treated EGCs *versus* respective control EGCs, and §P < 0.01, TcdB-treated EGCs at 6 or 13 days *versus* control EGCs at 48 h, Student's *t*-test. (D) Effect of TcdB treatment on catalase (CAT) activity expressed as μmol H_2O_2/min/10^6 cells.
In A and D, Data are the mean ± SEM from three different experiments. **P < 0.0001, *P < 0.05 TcdB-treated EGCs *versus* respective control EGCs, Student's *t*-test.

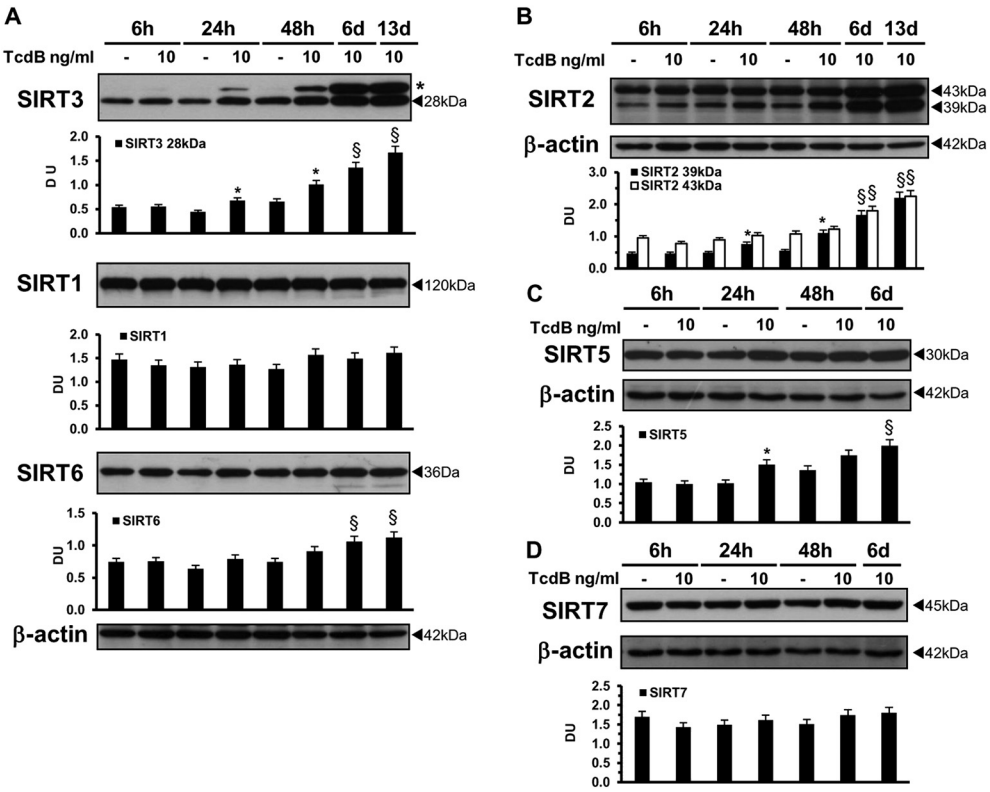

Fig. 8. Expression of SIRTs in TcdB-induced EGC senescence.

Lysates from control and TcdB-treated EGCs prepared at the times indicated were subjected to SDS-PAGE. (A) The filter was probed with anti-SIRT3, stripped, and probed with anti-β-actin, then the filter was stripped and cut to around 70 kDa to probe the bottom section with anti-SIRT6 and top section with anti-SIRT1. (B) The filter was probed with anti-SIRT2, stripped, and probed with anti-β-actin. (C) The filter was cut around 65 kDa to probe the bottom with anti-SIRT5 then stripped and probed with anti-β-actin. (D) The filter was probed with anti-SIRT7, stripped, and probed with anti-β-actin.

The graphs represent the densitometric analysis of each protein relative to β-actin. *P < 0.01, TcdB-treated EGCs *versus* respective control EGCs, and §P < 0.01, TcdB-treated EGCs at 6 or 13 days *versus* control EGCs at 48 h, Student's *t*-test. Star in A denoted a unknown band.

4. Discussion

This study contributes to the knowledge of new effects of TcdB in EGCs, an issue that could be relevant to chronic inflammation and tumorigenesis. Our key novel finding is that EGCs surviving the intoxication by TcdB undergo cellular senescence. Cellular senescence state occurs in response to endogenous and exogenous stressors, including the genotoxic and chemicals [13–20]. To date only a few studies highlight the role of bacterial toxins in the induction of senescence [25–30], and these studies are mainly focused on bacteria that cause limited infections [25–30], while no information is available on toxins of *C. difficile*, which causes a 15–25% of all opportunistic gastrointestinal infections [1–5].

The demonstration of TcdB-induced senescence in EGCs is very important because, according to recent studies that have found a significant epidemiological correlation between CDI and the onset of IBS and a possible epidemiological correlation with IBD [11,12], we speculated that after CDI the survival of altered EGCs could have functional consequences such as IBS [10], an hypothesis enforced by involvement of cellular senescence in several gastrointestinal diseases [32,33]. In fact, senescence, initially considered a barrier to tumor development, is now considered a potentially dangerous status because senescent cells secrete extremely active molecules that induce a persistent inflammatory environment, transfer senescence to bystander cells, and also promotes the proliferation of pre-neoplastic cells [13,14,17,31–33].

We interpreted as senescence the TcdB-induced phenotype in EGCs based on the following markers [13–22,31,33]: long-term and irreversible cell-cycle arrest, positivity for SA-β-Gal, flat morphology, persistent DNA damage evidenced by early phosphorylation of ATM and increased of γH2AX, overexpression of p27, hypophosphorylation of pRB, downregulation of c-Myc, cyclin B1, cdc2, and phosphorylated-cdc2.

TcdB at 10 ng/ml, as we have previous demonstrated [9], induced in EGC already at 1.5 h a strong glucosylation of Rac1 which persisted unchanged also at 13 days, indicative of a key event in induction of EGC senescence by TcdB.

Similar to what described in other models of senescence [13–17,25,28,30,38], we found early and persistent γH2AX foci, indicative of DNA damage, but not the formation of SAHF. However, SAHF and senescence are not always coupled; indeed, several studies have shown that senescence can occur in the absence of SAHF formation and, of note, SAHF formation is cell-type and stimulus dependent [13]. The strong induction of γH2AX very early after TcdB treatment (6 h), before the acquisition of the senescent phenotype is associated also with induction of DNA damage by TcdB in EGC because it is preceded by phosphorylation of the kinase ATM, that occurs already 1.5 h.

The classical senescence-inducing pathways p16/pRb and p53/p21 [13–24] do not play key roles in our model. In fact, we found that p16 expression levels sharply decreased from 48 h to 13 days. Consequently, pRb hypophosphorylation observed in TcdB-treated EGC is not p16-dependent but it could be due to inactivation of a CDK, which, in turn, is affected by p27 increase. Also, p21 does not play a key role in the induction of senescence, since its expression was significantly increased only at 6 and 13 days when EGCs have already acquired senescent phenotype, suggesting that p21 increase is involved in the maintenance of senescence state, as reported in other models [13–22].

Since we have used rat-transformed EGCs [35], even though these are considered equal to rat primary EGCs [35,42] and have functional properties similar to human EGCs [42], we have checked whether in EGCs the p53 pathway is still functional by inducing DNA damage with etoposide and looking at the phosphorylation and stabilization of p53 [43–45]. Our results demonstrating a dose-dependent phosphorylation and stabilization of p53 in EGCs at 6 h after etoposide treatment indicate that the p53 pathway is functional in EGCs and allow us to exclude the involvement p53/p21 axis in TcdB induction of EGC senescence.

Concerning the role of the senescence-inducing pathway PTEN/p27 [13–24] in our model, the p27 plays a central role, as indicated by its early and persistent strong increase, whereas PTEN seems not involved, because its expression does not change at all times examined. Therefore, in TcdB-induced EGC senescence the early and irreversible exit from cell-cycle was mediated by early and persistent p27

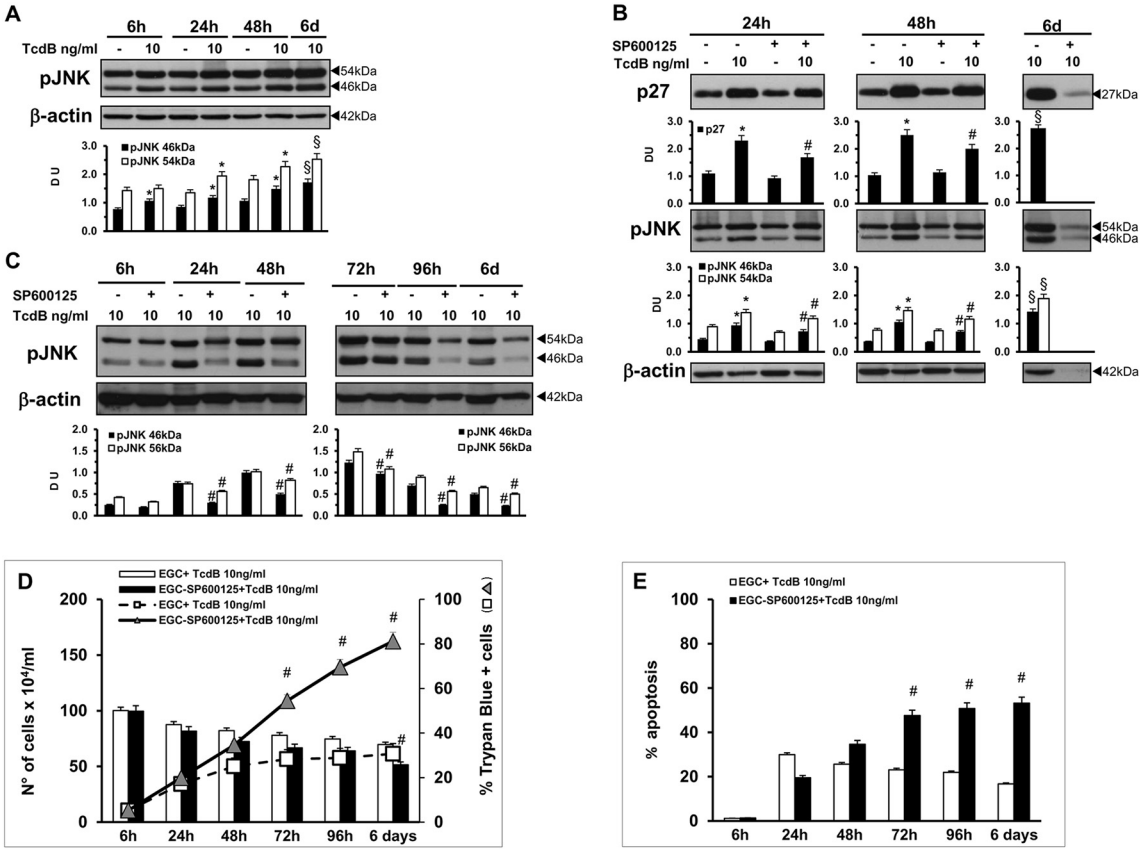

Fig. 9. Activation of JNK in TcdB-induced EGC senescence.

(A) Lysates from control and TcdB-treated EGCs prepared at the times indicated were subjected to SDS-PAGE. Then, the filter was probed with anti-pJNK, stripped, and probed with anti-β-actin. (B) Lysates from control and TcdB-treated EGCs, pre-treated or not for 1 h with 10 μM SP600125, prepared at the times indicated, were subjected to SDS-PAGE. The sample in the filters derived from the same experiment and blots are processed in parallel. The filters were cut to around 35 kDa to probe the bottom sections with anti-p27, and the top sections with anti-pJNK, then with anti-β-actin after stripping. (C) Lysates from TcdB-treated EGCs, pre-treated or not for 1 h with 10 μM SP600125, prepared at the times indicated, were subjected to SDS-PAGE. The sample in the filters derived from the same experiment and blots are processed in parallel. The filters were probe with anti-pJNK, then with anti-β-actin after stripping. (D, E) TcdB-treated EGCs, pre-treated or not for 1 h with 10 μM SP600125, were recovered at the times indicated. In (D) was determined the total cell number (histogram) and the percentage of trypanblue positive cells (lines with square or triangle), in (E) was determined the apoptosis by measuring the percentage of hypodiploid nuclei by flow cytometry. Treating control EGCs with SP600125 for the same time did not induce any effect (data not shown). Data are the mean ± standard deviation of three experiments performed in triplicate.

The graphs in A–C represent the densitometric analysis of each protein relative to β-actin $^{*}P < 0.01$, TcdB-treated EGCs *versus* respective control EGCs, and $^{\S}P < 0.01$, TcdB-treated EGCs at 6 days *versus* control EGCs at 48 h, $^{\#}P < 0.01$, TcdB-treated EGCs pre-treated with SP600125 *versus* TcdB-treated EGCs non-treated with inhibitor, Student's *t*-test. In D and E, $^{\#}P < 0.01$, TcdB-treated EGCs pre-treated with SP600125, versus TcdB-treated EGCs non-treated with inhibitor, Student's t-test.

overexpression, in association with early and persistent downregulation of cyclin B1, total cdc2, and phosphorylated-cdc2 (Tyr15 and Thr161), a cyclin and a CDK crucial for the checkpoint arrest of cell-cycle in G2/M [9,21]. Moreover, the phosphorylated-cdc2 Tyr15 shows an accumulation of the inactive hyperphosphorylated form of cdc2 Tyr 15 that is consistent with the G2 arrest.

According to the evidence that suppression of c-Myc induces cellular senescence in various cell types, because c-Myc promotes cell-cycle reentry and proliferation through inhibition of p21 and p27 expression [16,20,29,41], we found that TcdB induces early (6 h) and persistent downregulation of c-Myc which may allow p27 upregulation.

The finding that TcdB-induced senescence occurs by upregulation of p27, without involving p16/pRb and p53/p21 pathways, is in agreement with several studies that demonstrate induction of senescence by p27 upregulation in the absence of p16 and p21 upregulation, or in p16 and/or p21 knockout cells, thus indicating that p27 is able and sufficient by itself to induce senescence [13–16,20–24,46]. Moreover, in our model the induction of senescence without involving p16/pRb and p53/p21 pathways is in line with the evidence that, in contrast to the majority of senescence model that are characterized by cell-cycle exit at G1 phase, where p16 and p21 play a key role [18], in TcdB-treated EGCs cell-cycle exit occurs early (6 h) with arrest in G1 and G2, and disappearance of S phase.

Although the mechanisms leading to p27 upregulation are not completely defined, due to very complex regulation of p27 expression and functions, it is well known that p27 expression is post-translationally regulated *via* proteasome-dependent degradation by the SCF ubiquitin ligase complex, where the expression of the major determinant SKP2 is inversely proportional to p27 levels [41,56]. Since SKP2 levels do not change in TcdB-treated EGCs at all times examined (data not shown), in our model p27 overexpression is not attributable to SKP2 downregulation.

The expression of p27 and, more generally senescence, are also controlled by SIRTs, JNK, and AKT, by regulation of FOXO and transcription of its target genes (*e.g.* p27, MnSOD and catalase), through deacetylation (SIRTs), nuclear import and activation (JNK) and nuclear exclusion (AKT) [15,19,20,38,49–53].

Our demonstration that SIRT2 and SIRT3 were strongly overexpressed from 48 h to 13 days, and SIRT5 and SIRT6 at 6 and 13 days, indicates that SIRTs in our model were not involved in early p27

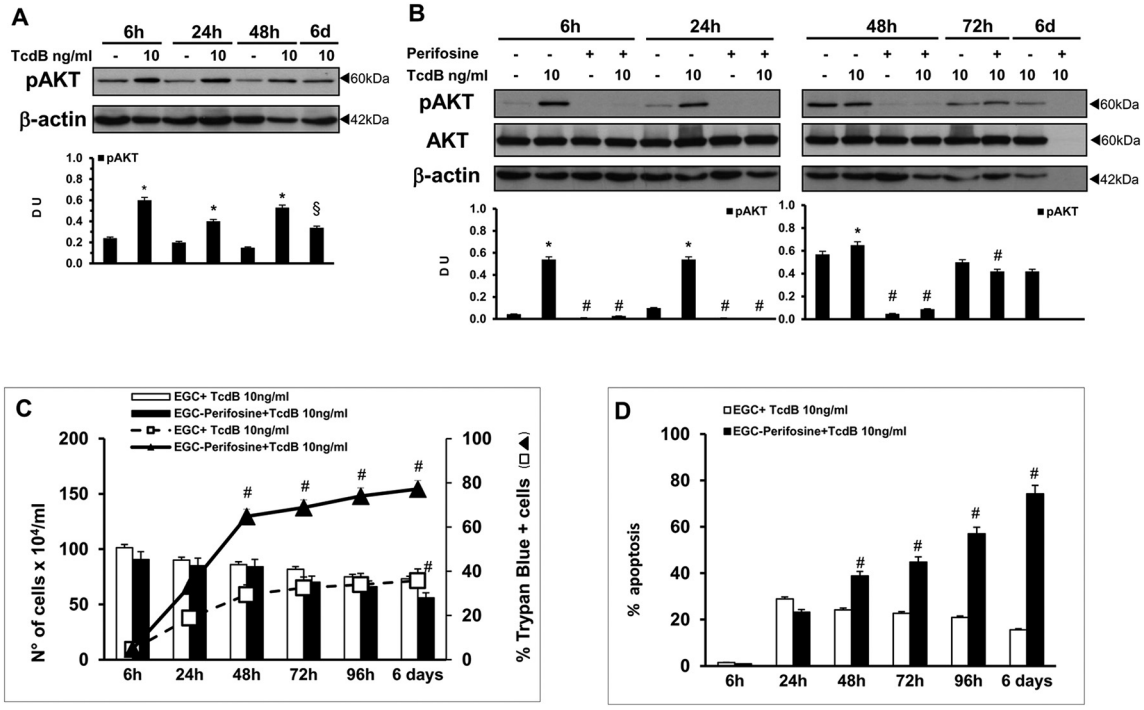

Fig. 10. Activation of AKT in TcdB-induced EGC senescence.

(A) Lysates from control and TcdB-treated EGCs prepared at the times indicated were subjected to SDS-PAGE. Then the filter was probed with anti-phospho-AKT (Ser473; pAKT), stripped, and probed with anti-β-actin. (B) Lysates from control and TcdB-treated EGCs, pre-treated or not for 1 h with 40 μM perifosine, prepared at the times indicated, were subjected to SDS-PAGE. The sample in the filters derived from the same experiment and blots are processed in parallel. The filters were probe with anti-pAKT, stripped, and probed with anti-β-actin, then with anti-AKT after stripping. The graphs represent the densitometric analysis of pAKT relative to β-actin. (C, D) TcdB-treated EGCs, pre-treated or not for 1 h with 40 μM perifosine, were recovered at the times indicated. In (C) was determined the total cell number (histogram) and the percentage of trypan blue positive cells (lines with square or triangle); in (D) was determined the apoptosis by measuring the percentage of hypodiploid nuclei by flow cytometry. Treating control EGCs with perifosine, for the same time did not induce any effect (data not shown). Data are the mean ± standard deviation of three experiments performed in triplicate.

In A and B, *P < 0.01, TcdB-treated EGCs *versus* respective control EGCs, and §P < 0.01, TcdB-treated EGCs at 6 days *versus* control EGCs at 48 h, $^{\#}$P < 0.01, TcdB-treated EGCs pre-treated with perifosine, *versus* TcdB-treated EGCs non-treated with inhibitor, Student's *t*-test. In C and D, $^{\#}$P < 0.01, TcdB-treated EGCs pre-treated with perifosine, versus TcdB-treated EGCs non-treated with inhibitor, Student's t-test.

increases, cell-cycle arrest and senescence induction but rather seem contribute to maturation and maintenance of senescence state, since senescence is a dynamic status progressively acquired and maintained [13,21]. Furthermore, the observation that SIRT2 and SIRT3 increase is strictly correlated with the decrease of intracellular ROS levels and overexpression of the antioxidant MnSOD suggest that in TcdB-induced senescence, SIRTs contribute also to stabilize the senescence state by triggering an antioxidant response to antagonize the lethal effects of high ROS levels, thus favouring EGCs survival. This is supported by the knowledge's that SIRT3 is mainly involved in inhibition of mitochondrial ROS production, induction of antioxidant response and cell survival pathway, while SIRT2 is mainly involved in the control of cell-cycle progression but contribute also in antagonize ROS increase [49–51]. To our knowledge this is the first demonstration of SIRT2 and SIRT3 involvement in senescence induced by a bacterial toxin. However, further studies are needed to understand the role of SIRT in TcdB-induced EGCs senescence and the mechanism(s) responsible of SIRTs overexpression.

The early and persistent activation of JNK induced by TcdB in EGCs, together with the demonstration that JNK inhibitor (SP600125) reduced p27 expression at 24 and 48 h but induced cell death by apoptosis progressively from 48 h to 6 days, indicate that in line with other models [14,15,19,29,47], in our model JNK is partially involved in the regulation of p27 expression and contribute to the survival of EGCs after TcdB treatment. In particular JNK activation is involved to make the choice between apoptosis or senescence that seems to be occurring between 48 and 72 h. The early AKT activation that persisted until 6 days together with the demonstration that the AKT inhibitor (perifosine) [54,55], induced cell death by apoptosis indicate that AKT plays a key role in induction of senescence by favouring survival of TcdB-treated EGCs and in particular to make the choice between apoptosis or senescence.

One of the stress factors frequently implicated in senescence development is the increase of intracellular ROS [14–16,20,25,29,30,46]. Our previous demonstration that TcdB induces in EGCs an increase of intracellular ROS [47] suggested that ROS could be responsible for TcdB-induced EGC senescence. However, the evidence that intracellular ROS levels increase until 48 h and go back to the level of control cells at 6 days, together with the observation that NAC does not reduce the percentage of SA-β-Gal positive cells, indicates that ROS do not play a key role in TcdB-induced EGC senescence. Furthermore, decrease of ROS could be due to upregulation of SIRTs and activation of JNK which trigger an antioxidant response mediated by increase of catalase activity at 24 and 48 h and of MnSOD expression between 48 h and 13 days.

Overall, our data show that induction of senescence by TcdB in EGCs shares with senescence induced by other bacterial toxins [25–30] persistent DNA damage and ROS production but differently from other bacterial toxins, ROS is not involved in senescence induction. In addition, in our model cell-cycle arrest occurs both at G1 and G2 phases and the permanent arrest of cell-cycle is not executed by p16 and p21, but by p27.

In conclusion, this study shows for the first time that TcdB induces senescence in EGCs, key cells in regulation of gastrointestinal tract

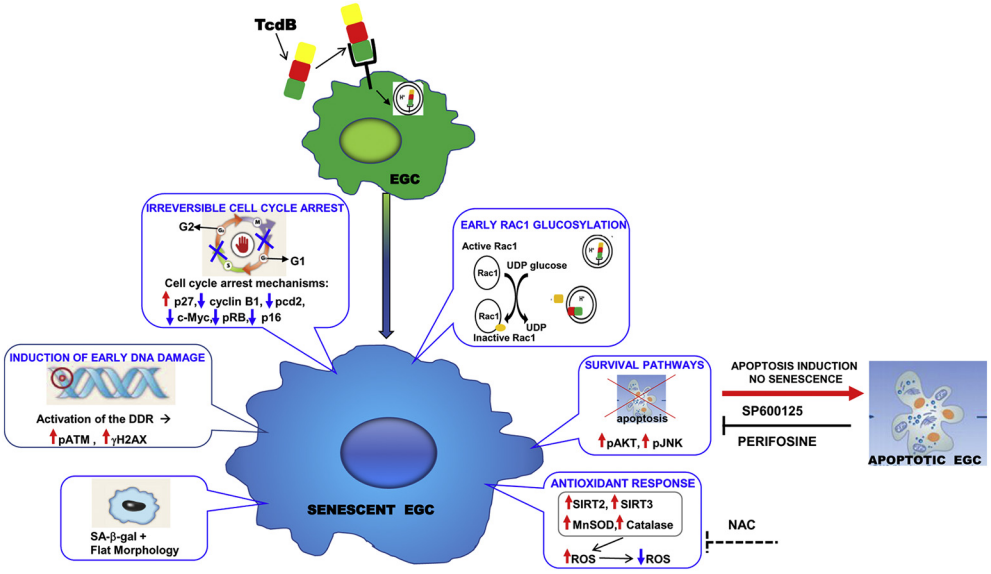

Fig. 11. Schematic diagram of main events of TcdB-induced EGC senescence.
TcdB induces in EGCs a senescence phenotype, which is dependent on p27 overexpression and activation of AKT and JNK, but independent on the p16/pRB and p53/p21 pathways as well as ROS.
In callout are reported the main events induced by TcdB.
SP600125 and perifosine inhibit TcdB-induced EGC senescence favouring EGC apoptosis.
NAC does not inhibit TcdB-induced EGC senescence.
Red arrows indicate increase of expression/phosphorylation. Blue arrows indicate decrease of expression/phosphorylation.

physiology and pathology, and the senescence is characterized by: irreversible cell-cycle arrest, SA-β-Gal positivity, flat morphology, early and persistent DNA damage (ATM and H2AX phosphorylation), p27 overexpression, pRB hypophosphorylation, c-Myc, cyclin B1, cdc2 and phosphorylated-cdc2 downregulation, SIRT2 and SIRT3 overexpression (Fig. 11). TcdB-induced EGC senescence is dependent by Rac1 glucosylation, JNK and AKT activation but independent on the p16 and p53/p21 pathways as well as ROS production (Fig. 11). If we extrapolate our *in vitro* data to CDI *in vivo*, namely whether after CDI some EGCs become senescent, a new field of study on long-term consequences of CDI could be opened with all the known implications about the pathological effects of senescence related to persistent inflammation, immune suppression, and tumor induction.

Author contributions

K.F.; conceived and devised the study, designed experiments and analysis; performed the experiments, analyzed the data, wrote and revised the manuscript for important intellectual content. L.M. and M.D.: performed experiments, analyzed the data, and performed statistical analysis. P.S. and C.P.: performed immunofluorescence experiments, analyzed the data and performed statistical analysis. L.C.: critically revised the manuscript. A.M., M.C., and A.S.: performed statistical analysis and critically revised the manuscript. P.M.: supervised the research and revised the manuscript for important intellectual content. G.B.: supervised the research, revised the manuscript for important intellectual content and obtained funding.

All authors degree to the submission of the manuscript and have approved the present version.

Competing interests

The authors declare no competing interests.

Transparency document

The Transparency document associated with this article can be found, in online version.

Acknowledgments

We are greatly indebted to Sofar S.P.A. company for its generous unrestricted support. This work was supported by a Project from the Department of Medicine (bando 2015) awarded to Professor Gabrio Bassotti. This work was supported by a Project from the Department of Experimental Medicine (bando 2017) awarded to Doctor Katia Fettucciari.

This research did not received specific grant from funding agency in the public, commercial or not-for profit sectors.

The funders had no role in study design, data collection and interpretation, or the decision to submit the work for publication.

References

[1] K.A. Davies, H. Ashwin, C.M. Longshaw, D.A. Burns, G.L. Davis, M.H. Wilcox, EUCLID Study Group, Diversity of *Clostridium difficile* PCR ribotypes in Europe: results from the European, multicentre, prospective, biannual, point-prevalence study of *Clostridium difficile* infection in hospitalised patients with diarrhoea (EUCLID), 2012 and 2013, Euro Surveill. 21 (2016) 30294, https://doi.org/10.2807/1560-7917.ES.2016.21.29.30294.

[2] A.N. Ananthakrishnan, *Clostridium difficile* infection: epidemiology, risk factors and management, Nat. Rev. Gastroenterol. Hepatol. 8 (2011) 17–26, https://doi.org/10.1038/nrgastro.2010.190.

[3] K. Aktories, C. Schwan, T. Jank, *Clostridium difficile* toxin biology, Annu. Rev. Microbiol. 71 (2017) 281–307, https://doi.org/10.1146/annurev-micro-090816-093458.

[4] X. Sun, T. Savidge, H. Feng, The enterotoxicity of *Clostridium difficile* toxins, Toxins 2 (2010) 1848–1880, https://doi.org/10.3390/toxins2071848.

[5] R.N. Pruitt, D.B. Lacy, Toward a structural understanding of *Clostridium difficile* toxins A and B, Front. Cell. Infect. Microbiol. 2 (2012) 28, https://doi.org/10.3389/fcimb.2012.00028.

[6] V. Grubišić, B.D. Gulbransen, Enteric glia: the most alimentary of all glia, J. Physiol. 595 (2017) 557–570, https://doi.org/10.1113/JP271021.

[7] M. Neunlist, M. Rolli-Derkinderen, R. Latorre, L. Van Landeghem, E. Coron, P. Derkinderen, R. De Giorgio, Enteric glial cells: recent developments and future directions, Gastroenterology 147 (2014) 1230–1237, https://doi.org/10.1053/j.gastro.2014.09.040.

[8] G. Bassotti, V. Villanacci, Can "functional" constipation be considered as a form of enteric neuro-gliopathy? Glia 59 (2011) 345–350, https://doi.org/10.1002/glia.21115.

[9] K. Fettucciari, P. Ponsini, D. Gioè, L. Macchioni, C. Palumbo, E. Antonelli, S. Coaccioli, V. Villanacci, L. Corazzi, P. Marconi, G. Bassotti, Enteric glial cells are susceptible to *Clostridium difficile* toxin B, Cell. Mol. Life Sci. 74 (2017) 1527–1551, https://doi.org/10.1007/s00018-016-2426-4.

[10] G. Bassotti, L. Macchioni, L. Corazzi, P. Marconi, K. Fettucciari, *Clostridium difficile*-related postinfectious IBS: a case of enteroglial microbiological stalking and/or the solution of a conundrum? Cell. Mol. Life Sci. 75 (2018) 1145–1149, https://doi.org/10.1007/s00018-017-2736-1.

[11] R.L. Gutiérrez, M.S. Riddle, C.K. Porter, Increased risk of functional gastrointestinal sequelae after *Clostridium difficile* infection among active duty United States military personnel (1998–2010), Gastroenterology 149 (2015) 1408–1414, https://doi.org/10.1053/j.gastro.2015.07.059.

[12] A. Wadhwa, M.F. Al Nahhas, R.A. Dierkhising, R. Patel, P. Kashyap, D.S. Pardi, S. Khanna, M. Grover, High risk of post-infectious irritable bowel syndrome in patients with *Clostridium difficile* infection, Aliment. Pharmacol. Ther. 44 (2016) 576–582, https://doi.org/10.1111/apt.13737.

[13] J. Campisi, Aging, cellular senescence, and cancer, Annu. Rev. Physiol. 75 (2013) 685–705, https://doi.org/10.1146/annurev-physiol-030212-183653.
[14] T. Kuilman, C. Michaloglou, W.J. Mooi, D.S. Peeper, The essence of senescence, Genes Dev. 24 (2010) 2463–2479, https://doi.org/10.1101/gad.1971610.
[15] I. Fridlyanskaya, L. Alekseenko, N. Nikolsky, Senescence as a general cellular response to stress: a mini-review, Exp. Gerontol. 72 (2015) 124–128, https://doi.org/10.1016/j.exger.2015.09.021.
[16] I. Ben-Porath, R.A. Weinberg, The signals and pathways activating cellular senescence, Int. J. Biochem. Cell Biol. 37 (2005) 961–976, https://doi.org/10.1016/j.biocel.2004.10.013.
[17] R. Salama, M. Sadaie, M. Hoare, M. Narita, Cellular senescence and its effector programs, Genes Dev. 28 (2014) 99–114, https://doi.org/10.1101/gad.235184.113.
[18] V. Gire, V. Dulic, Senescence from G2 arrest, revisited, Cell Cycle 14 (2015) 297–304, https://doi.org/10.1080/15384101.2014.1000134.
[19] J. Maruyama, I. Naguro, K. Takeda, H. Ichijo, Stress-activated MAP kinase cascades in cellular senescence, Curr. Med. Chem. 16 (2009) 1229–1235.
[20] N.V. Petrova, A.K. Velichko, S.V. Razin, O.L. Kantidze, Small molecule compounds that induce cellular senescence, Aging Cell 10 (2016) 999–1017, https://doi.org/10.1111/acel.12518.
[21] F. Bringold, M. Serrano, Tumor suppressors and oncogenes in cellular senescence, Exp. Gerontol. 35 (2000) 317–329.
[22] S.H. Park, J.S. Lim, K.L. Jang, All-trans retinoic acid induces cellular senescence via upregulation of p16, p21, and p27, Cancer Lett. 310 (2011) 232–239, https://doi.org/10.1016/j.canlet.2011.07.009.
[23] K. Alexander, P.W. Hinds, Requirement for p27(KIP1) in retinoblastoma protein-mediated senescence, Mol. Cell. Biol. 21 (2001) 3616–3631, https://doi.org/10.1128/MCB.21.11.3616-3631.2001.
[24] M. Collado, R.H. Medema, I. Garcia-Cao, M.L. Dubuisson, M. Barradas, J. Glassford, C. Rivas, B.M. Burgering, M. Serrano, E.W. Lam, Inhibition of the phosphoinositide 3-kinase pathway induces a senescence-like arrest mediated by $p27^{Kip1}$, J. Biol. Chem. 275 (2000) 21960–21968, https://doi.org/10.1074/jbc.M000759200.
[25] T. Secher, A. Samba-Louaka, E. Oswald, J.P. Nougayrède, *Escherichia coli* producing colibactin triggers premature and transmissible senescence in mammalian cells, PLoS One 8 (2013) e77157, , https://doi.org/10.1371/journal.pone.0077157.
[26] M. Muller, Premature cellular senescence induced by pyocyanin, a redox-active *Pseudomonas aeruginosa* toxin, Free Radic. Biol. Med. 41 (2006) 1670–1677, https://doi.org/10.1016/j.freeradbiomed.2006.09.004.
[27] M. Muller, Z. Li, P.K.M. Maitz, Pseudomonas pyocyanin inhibits wound repair by inducing premature cellular senescence: role for p38 mitogen-activated protein kinase, Burns 35 (2009) 500–508, https://doi.org/10.1016/j.burns.2008.11.010.
[28] H. Blazkova, K. Krejcikova, P. Moudry, T. Frisan, Z. Hodny, J. Bartek, Bacterial intoxication evokes cellular senescence with persistent DNA damage and cytokine signalling, J. Cell. Mol. Med. 14 (2010) 357–367, https://doi.org/10.1111/j.1582-4934.2009.00862.x.
[29] I.S. Kwon, J. Kim, D.K. Rhee, B.O. Kim, S. Pyo, Pneumolysin induces cellular senescence by increasing ROS production and activation of MAPK/NF-κB signal pathway in glial cells, Toxicon 129 (2017) 100–112, https://doi.org/10.1016/j.toxicon.2017.02.017.
[30] F. Grasso, T. Frisan, Bacterial genotoxins: merging the DNA damage response into infection biology, Biomol. Ther. 5 (2015) 1762–1782, https://doi.org/10.3390/biom5031762.
[31] P. Hinds, J. Pietruska, Senescence and tumor suppression, F1000Res 6 (2017) 2121, https://doi.org/10.12688/f1000research.11671.1.
[32] J.D. Penfield, M. Anderson, L. Lutzke, K.K. Wang, The role of cellular senescence in the gastrointestinal mucosa, Gut Liver 7 (2013) 270–277, https://doi.org/10.5009/gnl.2013.7.3.270.
[33] N. Frey, S. Venturelli, L. Zender, M. Bitzer, Cellular senescence in gastrointestinal diseases: from pathogenesis to therapeutics, Nat. Rev. Gastroenterol. Hepatol. 15 (2018) 81–95, https://doi.org/10.1038/nrgastro.2017.146.
[34] G.P. Dimri, X. Lee, G. Basile, M. Acosta, G. Scott, C. Roskelley, E.E. Medrano, M. Linskens, I. Rubelj, O. Pereira-Smith, M. Peacocke, J. Campisi, A biomarker that identifies senescent human cells in culture and in aging skin in vivo, Proc. Natl. Acad. Sci. U. S. A. 92 (1995) 9363–9367, https://doi.org/10.1073/pnas.92.20.9363.
[35] A. Rühl, J. Trotter, W. Stremmel, Isolation of enteric glia and establishment of transformed enteroglial cell lines from the myenteric plexus of adult rat, Neurogastroenterol. Motil. 13 (2001) 95–106.
[36] B.I. Gerashchenko, E.I. Azzam, R.W. Howell, Characterization of cell-cycle progression and growth of WB-F344 normal rat liver epithelial cells following gamma-ray exposure, Cytometry A 61 (2004) 134–141, https://doi.org/10.1002/cyto.a.20065.
[37] H.E. Aebi, Catalase, in: H.U. Bergmeyer (Ed.), Methods of Enzymatic Analysis, Verlag Chemie, Weinheim, 1983, pp. 273–286.
[38] M.K. Eren, A. Kilincli, Ö. Eren, Resveratrol induced premature senescence is associated with DNA damage mediated SIRT1 and SIRT2 down-regulation, PLoS One 10 (2015) e0124837, , https://doi.org/10.1371/journal.pone.0124837.
[39] J. Huelsenbeck, S. Dreger, R. Gerhard, H. Barth, I. Just, H. Genth, Difference in the cytotoxic effects of toxin B from *Clostridium difficile* strain VPI 10463 and toxin B from variant *Clostridium difficile* strain 1470, Infect. Immun. 75 (2007) 801–809, https://doi.org/10.1128/IAI.01705-06.
[40] H. Genth, J. Huelsenbeck, B. Hartmann, F. Hofmann, I. Just, R. Gerhard, Cellular stability of Rho-GTPases glucosylated by *Clostridium difficile* toxin B, FEBS Lett. 580 (2006) 3565–3569, https://doi.org/10.1016/j.febslet.2006.04.100.
[41] P. Hydbring, A. Castell, L.G. Larsson, MYC modulation around the CDK2/p27/SKP2 axis, Genes 8 (2017) E174, , https://doi.org/10.3390/genes8070174.
[42] R. Soret, S. Coquenlorge, F. Cossais, G. Meurette, M. Rolli-Derkinderen, M. Neunlist, Characterization of human, mouse, and rat cultures of enteric glial cells and their effect on intestinal epithelial cells, Neurogastroenterol. Motil. 25 (2013) e755–e764, https://doi.org/10.1007/s00018-008-8296-7.
[43] N.O. Karpinich, M. Tafani, R.J. Rothman, M.A. Russo, J.L. Farber, The course of etoposide-induced apoptosis from damage to DNA and p53 activation to mitochondrial release of cytochrome c, J. Biol. Chem. 277 (2002) 16547–16552, https://doi.org/10.1074/jbc.M110629200.
[44] E. Müllers, H. Silva Cascales, H. Jaiswal, A.T. Saurin, A. Lindqvist, Nuclear translocation of Cyclin B1 marks the restriction point for terminal cell cycle exit in G2 phase, Cell Cycle 13 (2014) 2733–2743, https://doi.org/10.4161/15384101.2015.945831.
[45] M.F. Lavin, N. Gueven, The complexity of p53 stabilization and activation, Cell Death Differ. 13 (2006) 941–950, https://doi.org/10.1038/sj.cdd.4401925.
[46] I. Lee, C. Park, W.K. Kang, Knockdown of inwardly rectifying potassium channel Kir2.2 suppresses tumorigenesis by inducing reactive oxygen species-mediated cellular senescence, Mol. Cancer Ther. 9 (2010) 2951–2959, https://doi.org/10.1158/1535-7163.MCT-10-0511.
[47] L. Macchioni, M. Davidescu, K. Fettucciari, M. Petricciuolo, L. Gatticchi, D. Gioè, V. Villanacci, M. Bellini, P. Marconi, R. Roberti, G. Bassotti, L. Corazzi, Enteric glial cells counteract *Clostridium difficile* Toxin B through a NADPH oxidase/ROS/JNK/caspase-3 axis, without involving mitochondrial pathways, Sci. Rep. 7 (2017) 45569, https://doi.org/10.1038/srep45569.
[48] L. He, T. He, S. Farrar, L. Ji, T. Liu, X. Ma, Antioxidants maintain cellular redox homeostasis by elimination of reactive oxygen species, Cell. Physiol. Biochem. 44 (2017) 532–553, https://doi.org/10.1159/000485089.
[49] S. Ghosh, Z. Zhou, SIRTain regulators of premature senescence and accelerated aging, Protein Cell 6 (2015) 322–333, https://doi.org/10.1007/s13238-015-0149-1.
[50] M. Wątroba, D. Szukiewicz, The role of sirtuins in aging and age-related diseases, Adv. Med. Sci. 61 (2016) 52–62, https://doi.org/10.1016/j.advms.2015.09.003.
[51] T. Anwar, S. Khosla, G. Ramakrishna, Increased expression of SIRT2 is a novel marker of cellular senescence and is dependent on wild type p53 status, Cell Cycle 15 (2016) 1883–1897, https://doi.org/10.1080/15384101.2016.1189041.
[52] H. Huang, D.J. Tindall, Dynamic FoxO transcription factors, J. Cell Sci. 120 (2007) 2479–2487, https://doi.org/10.1242/jcs.001222.
[53] Y. Xu, N. Li, R. Xiang, P. Sun, Emerging roles of the p38 MAPK and PI3K/AKT/mTOR pathways in oncogene-induced senescence, Trends Biochem. Sci. 39 (2014) 268–276, https://doi.org/10.1016/j.tibs.2014.04.004.
[54] S.B. Kondapaka, S.S. Singh, G.P. Dasmahapatra, E.A. Sausville, K.K. Roy, Perifosine, a novel alkylphospholipid, inhibits protein kinase B activation, Mol. Cancer Ther. 2 (2003) 1093–1103.
[55] L. de la Peña, W.E. Burgan, D.J. Carter, M.G. Hollingshead, M. Satyamitra, K. Camphausen, P.J. Tofilon, Inhibition of Akt by the alkylphospholipid perifosine does not enhance the radiosensitivity of human glioma cells, Mol. Cancer Ther. 5 (2006) 1504–1510, https://doi.org/10.1158/1535-7163.MCT-06-0091.
[56] J. Vervoorts, B. Lüscher, Post-translational regulation of the tumor suppressor p27(KIP1), Cell. Mol. Life Sci. 65 (2008) 3255–3264, https://doi.org/10.1007/s00018-008-8296-7.